Producing Crack-Free Colloid−Polymer Hybrid Gels by Tailoring Porosity

María J. Mosquera,*,† Mercedes Bejarano,† Nicolás de la Rosa-Fox,‡ and Luis Esquivias‡

Departamento de Química-Física, Facultad de Ciencias, and Departamento de Física de la Materia Condensada, Facultad de Ciencias, Universidad de Cádiz, 11510 Puerto Real, Spain

Received September 24, 2002. In Final Form: November 11, 2002

Several mixtures obtained by ultrasonic agitation of colloidal silica with a sol solution containing tetraethoxysilane (TEOS) were used to form crack-free monoliths. The dry gels that were submitted to mercury porosimetry showed differences in behavior according to the proportion of silica colloid in the gel. For low proportions, the mercury isostatic pressure exclusively induced an irreversible compaction of material, but intrusion occurred in gels with a high proportion of colloid. This permitted the evaluation of the textural properties of intruded gels, whereas the pressurization−depressurization paths, where intrusion was prevented, provided information about their compression behavior. Specimens exhibited elastic strain, followed by yield and plastic hardening. Bulk modulus was significantly reduced as the content of silica particles in the gel was increased. This was related to the increase in free volume of the network. The yield point, which characterizes the limit of the elastic region, was taken as a reference for estimating the maximum capillary pressure of drying; the inclusion of colloidal silica progressively reduced the maximum capillary pressure occurring during the drying for all samples except those containing the highest proportion of colloid (82%). This anomalous behavior was associated with low TEOS content, which complicates the formation of siloxane bonds. Textural properties determined by nitrogen adsorption confirmed the results obtained by porosimetry. Both porous volume and pore size were gradually increased in line with the colloid content. Therefore, we offer an effective means of tailoring the derived sol−gel porosity by increasing the proportion of colloidal silica, starting from a dense microporous material to achieve a mesoporous gel with a high pore volume and reduced capillary pressure.

Introduction

The sol−gel process is a very common method for manufacturing mesoporous materials, which find applications in fields as diverse as electronics,[1,2] catalysis,[3] molecular separations,[4] and even monumental conservation.[5,6] It is well-known that one of the main problems of the method is the occurrence of cracking during the drying process. This limitation has prevented the more widespread use of the sol−gel route for producing monoliths and films. Gel cracking[7] occurs as a result of stresses caused by the existence of a meniscus at the liquid−vapor interface, which generates a differential capillary pressure within the gel. This makes the network shrink until it becomes stiff enough to resist the stress imposed by capillary pressure. At this point the maximum capillary tension is reached; this value is given by the Young−Laplace equation, assuming that the pores are cylindrical. Then, the liquid−vapor interface progressively retreats into the structure of the gel until it disappears when the drying stage is completed. Equation 1 shows the Young−Laplace expression corresponding to cylindrical pores, where γ is the liquid−vapor tension, θ is the contact angle of liquid to pore wall, and r_p is the pore radius.

$$P_{max} = \frac{2\gamma_{LV}\cos\theta}{r_p} \quad (1)$$

Although there may be capillary pressure in the gel, if it were uniform, the network would be uniformly compressed, and there would be no cracking. Therefore, the stress that causes damage results from the pressure gradient across the network and not from the absolute value of the pressure. The gradient obviously increases at high liquid evaporation rates, so the most direct solution for avoiding cracking would be to let the liquid evaporate at a very low rate. Modification of network permeability is another key factor since a low permeability generates a high-pressure gradient.

It is obvious that any changes made to these parameters that tend to minimize the capillary pressure should increase the probability of monolithic gel formation. One alternative is to add drying control chemical additives (DCCA), the low surface tension of which acts to reduce capillary pressure.[8,9] Another efficient way of neutralizing the undesired effects of surface tension is to suppress the liquid−vapor interface. This is achieved by treating the gel in an autoclave under supercritical conditions for the solvent, taking care that the path of the thermal treatment

* Corresponding author. Tel: +34-956016331. Fax: +34-956016288. E-mail: mariajesus.mosquera@uca.es.

† Departamento de Química-Física.

‡ Departamento de Física de la Materia Condensada.

(1) Mezza, P., Phalippou, J.; Sempere, R. J. *Non-Cryst. Solids* **1999**, *243*, 75−79.

(2) Baskaran, S.; Liu, J.; Domansky K.; Kholer, N.; Li, X.; Coyle, C.; Fryxell, G. E.; Thevuthasan, S.; Williford, R. E. *Adv. Mater.* **2000**, *12*, 291−294.

(3) Maschmeyer, T. *Curr. Opin. Solid State Mater. Sci.* **1998**, *3*, 71−78.

(4) Davis, M. E. *Nature* **1993**, *364*, 391−393.

(5) Scherer, G. W.; Wheeler, G. E. In *Proceedings of the 4th International Symposium on the Conservation of Monuments in the Mediterranean*; Moropulou, Zezza, Kollias, Papachristodoulou, Eds.; Technical Chamber of Greece: Rhodes, Greece, 1997.

(6) Mosquera, M. J.; Pozo J. Esquivias, L.; Rivas, T.; Silva, B. *J. Non-Cryst. Solids* **2002**, *311*, 185−194.

(7) Scherer G. W. *J. Non-Cryst. Solids* **1992**, *147*, *148*, 363−374.

(8) Shiomi, H.; Kakimoto, C.; Nakahira, A. *J. Sol-Gel Sci. Technol.* **2000**, *19*, 759−763.

(9) Harreld, J. H.; Ebina, T.; Tsubo, N.; Stucky G. *J. Non-Cryst. Solids* **2002**, *298*, 241−251.

10.1021/la0265981 CCC: $25.00
Published on Web 12/31/2002

does not cross the equilibrium curve.[10] A recent strategy is the insertion into the wet gel network of removable entities that help to support the capillary stresses during the drying stage; these are finally eliminated by thermal or chemical treatment after the reinforcement of the solid network. The important advantage of this method is that these entities act as templates, generating a microstructure similar to the initial units. Consequently, the microstructure of nanoporous gels can easily be tailored as required.[11−13]

Since most of the methods described are based on modifications of drying conditions, they cannot, unfortunately, be adopted in applications when the sol is incorporated into a porous matrix that must dry at ambient conditions, as a prior step to gelling. This is the case of TEOS-based compounds used as stone consolidants in the conservation of monumental building. Their low viscosity enables them to penetrate deeply into the stone. Then, environmental moisture is enough to achieve the gelling inside the pore structure of the stone, giving a stable polymer with silicon−oxygen backbone similar to rock minerals. In fact, the initial focus of this work was specifically to obtain crack-free stone consolidants. However, the procedure described in the paper can be extended to the production of monoliths and films in general.

Some years ago, successful trials to obtain crack-free sintered gels with optical applications were carried out by including colloidal fumed silica particles in the gel.[14−17] It is clear that pores formed between these relatively large particles are also large and, in accordance with eq 1, capillary stress is reduced. Moreover, a large pore size generates high permeability values, thus reducing the pressure gradient across the network. In recent papers, Alié et al.[18−20] achieved the decrease of capillary stress by the addition of substituted alkoxides, such as 3-((2-aminoethyl)amino)propyltrimethoxysilane (EDAS), during the synthesis of silica gels; the EDAS acted as a nucleation agent leading to the formation of large silica particles in the gel. Merkel et al.[21] achieved the simultaneous increase of the permeability and selectivity of nanocomposite membranes, by dispersion of nanoscale silica particles in a glassy amorphous polymer.

In the specific case of TEOS-based stone consolidants, Scherer et al.[22−24] reduced shrinkage by adding colloidal oxide particles, such as silica, titania, or various pigments (oxides of iron, chrome, and cobalt). The result of this was that these novel gels did not crack during drying inside the stone. In addition, the porosity was increased, thus increasing the permeability and sorptivity of the treated stone. To avoid an undesirable increase of viscosity due to the aggregation of particles, these oxide powders were coated with nanometricsilica particles. Sols prepared in this way exhibited low viscosities and so readily penetrated the stone.

This paper describes an attempt to avoid cracking during drying of gels, by adding colloidal fumed silica (Aerosil OX-50) to TEOS, in varying proportions. We use mercury porosity for characterizing shrinkage behavior of gels under isostatic pressure of mercury. The compression curves provide interesting information about the drying process of the gels examined.

Additionally, we investigate the effect of colloid addition on the pore structure of gels by nitrogen adsorption−desorption and mercury porosimetry. Currently, many research projects in the sol−gel field are focused on producing materials with larger pore volume and pore size than those in standard dense microstructures of xerogels. Therefore, we extend the focus of the paper to the tailoring of the textural properties of the gels by the addition of silica particles. In its specific application as a stone consolidant, a serious limitation of a TEOS gel is that it completely closes the pores of the rocks, which must be avoided. The production of gels with a high pore volume is thus of considerable potential value. Clearly other requirements corresponding to consolidants, such as a low product viscosity to permit deep penetration into the stone and product transparency, must be taken into account.

Experimental Section

Synthesis of the Gels. Monolithic colloid−polymer hybrid gels containing various proportions of silica particles were prepared by following the synthesis method proposed by Toki et al.[16] The colloidal silica selected was Aerosil-OX-50 (Degussa) produced by hydrolyzing $SiCl_4$ with an oxygen−hydrogen flame. According to manufacturer's specifications, the product exhibits a low specific surface area of 50 m^2/g. The percentage by weight of SiO_2 particles to total SiO_2 was varied between 30, 54, 65, and 82. For comparison, a sol without addition of colloidal silica was produced by following the same preparation process. H_2O−TEOS−HCl were mixed in the mole ratio of 10:1:0.001. First, prehydrolysis was initiated by 5 min of exposure to ultrasonic agitation. The sonicated sols were stirred until the complete homogenization was achieved to ensure the total hydrolysis of TEOS. Next, the pH value of the sol was measured with a glass-electrode pH-meter and then 0.1 N ammonia solution was added until the pH reached 4.5. The mixture, which was poured into hermetically closed recipients, gelled at room temperature over a period of hours. Once the gellification was complete, the gels were dried in an oven at 50 °C. A pinhole aperture limited the drying rate. Gels were left in the oven until no change of weight was observed, which occurred in 2 weeks.

Mercury Intrusion Porosimetry. Monoliths from sols containing the different proportions of colloidal particles were subjected to mercury pressure in a Pascal 440 porosimeter from Fisons Instruments. Pressure was varied between 0.1 and 390 MPa. Corresponding paths of pressurization−depressurization were recorded in all cases. To investigate whether mercury intrusion occurs in network pores, specimen runs were compared with results of other specimens encapsulated in a rubber membrane, which prevents the entry of mercury. A rotary vacuum pump was used to extract the air from the membrane. To eliminate errors associated with the encapsulation, a blank of

(10) Brinker, C. J.; Scherer, G. W. *Sol−gel science, the physics and chemistry of sol−gel processing*; Academic Press: Boston, MA, 1990.
(11) McGrath, K. M.; Dabbs D. M.; Yao, N. I.; Aksay, A.; Gruner, S. M. *Science* **1997**, *277*, 552−556.
(12) Klotz, M.; Ayral, A.; Guizar, C.; Cot, L. *Bull. Korean Chem. Soc.* **1999**, *20*, 879−884.
(13) McGrath, K. M.; Dabbs, D.M.; Yao, N., Edler, K. J.; Aksay, I. A. Gruner, S. M. *Langmuir* **2000**, *16*, 398−406.
(14) Scherer, G. W.; Luong, J.C. *J. Non-Cryst. Solids* **1984**, *63*, 163−172.
(15) Clasen, R. *J. Non-Cryst. Solids* **1987**, *89*, 335−344.
(16) Toki, M.; Miyashita, S.; Takeuchi, T.; Kanbe, S.; Kochi A. *J. Non-Cryst. Solids* **1988**, *100*, 479−482.
(17) Okazaki, H.; Kitagawa, T.; Shibata, S.; Kimura, T. *J. Non-Cryst. Solids* **1990**, *116*, 87−92.
(18) Alié, C.; Pirard, R.; Lecloux, A. J.; Pirard, J. P. *J. Non-Cryst. Solids* **1999**, *246*, 216−228.
(19) Alié, C.; Benhaddou, A.; Pirard, R.; Lecloux, A. J.; Pirard, J. P. *J. Non-Cryst. Solids* **2000**, *270*, 77−90.
(20) Alié, C.; Ferauche, F.; Pirard, R.; Lecloux, A. J.; Pirard, J. P. *J. Non-Cryst. Solids* **2001**, *289*, 88−96.
(21) Merkel, T. C.; Freeman, B. D.; Spontak, R. J.; He, Z.;. Pinnau, I.; Meakin, P.; Hill, A. J. *Science* **2002**, *296*, 519−522.
(22) Scherer, G. W.; Flatt, R.; Wheeler, G. *MRS Bull.* **2001**, *26*, 44−50.
(23) Escalante, M. R.; Flatt, R.; Scherer, G. W.; Tsiourva, D.; Moropoulou, A. In *Protection and Conservation of the Cultural Heritage of the Mediterranean cities*; Galan, Zezza, Eds.; A. A. Balkema: The Netherlands, 2002.
(24) Escalante, M. R.; Valenza, J.; Scherer, G. W. In *Proceedings of the 9th International Congress on Deterioration and Conservation of Stone*; Fassina, Ed.; Venice, Italy, 2000; Elsevier Science B.V.: The Netherlands; Vol. 2, pp 459−465.

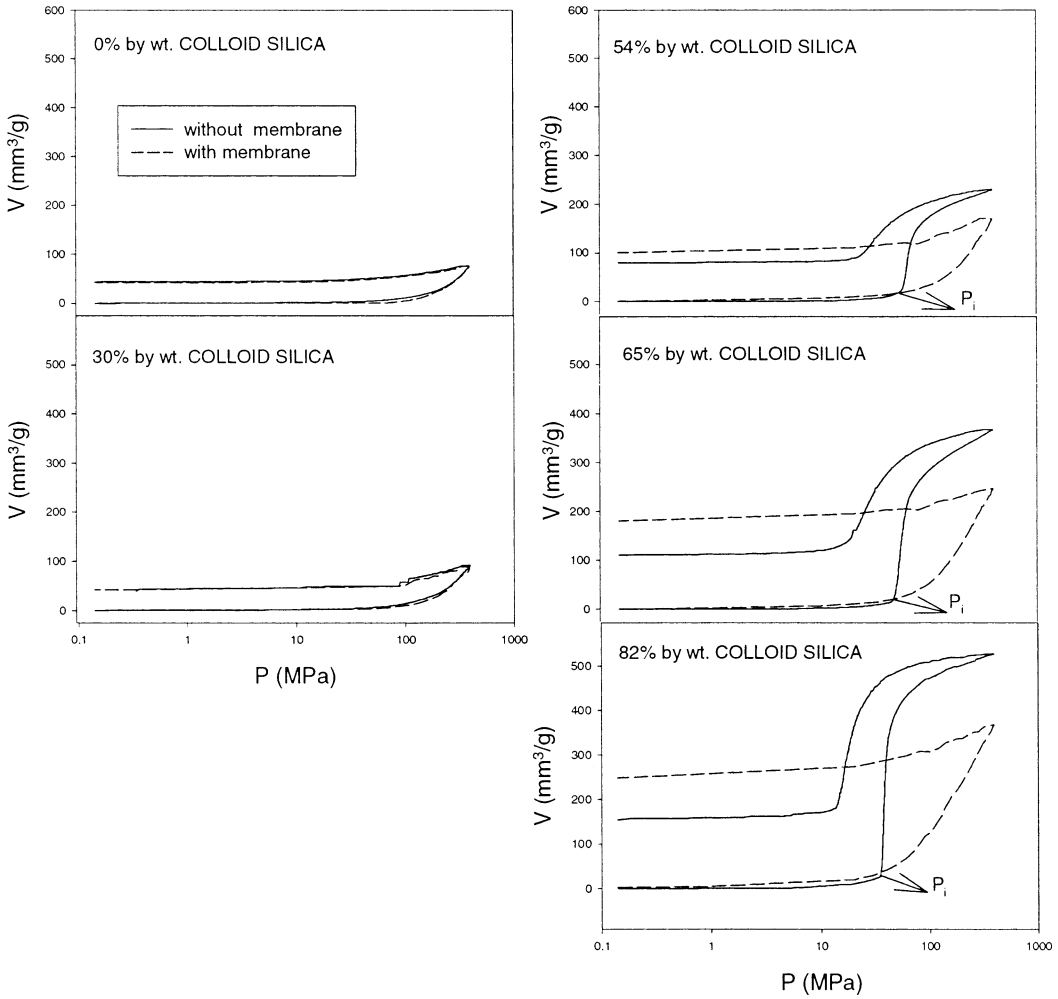

Figure 1. Mercury porosimetry curves: pressure vs volume variation. P_i is the pressure corresponding to the initial intrusion.

rubber membrane without sample was run, and the curve obtained was subtracted from all data corresponding to encapsulated samples. Moreover, sample weight was checked before and after the run as additional information about mercury intrusion. Weight information was also used to ensure that the encapsulated test was correct and intrusion was avoided.

In addition, each gel with a different proportion of silica was subjected to a sequential pressurization experiment. To prevent mercury intrusion in specimens where this may occur, these were previously encapsulated. A total of 10 cycles of sequential pressurization−depressurization were carried out without removing the specimen. The maximum pressure of each cycle was successively increased to the following values: 25, 50, 75, 100, 125, 150, 200, 250, 300, and 390 MPa.

Finally, the bulk densities of the gels were calculated from mass values and volume data, which were obtained from porosimetry. Similarly, data on volume variation after experiments where intrusion was prevented enabled the calculation of bulk density of the compacted networks.

Nitrogen Adsorption−Desorption. Gas physisorption was carried out in a Sorptomatic 1990 from Fisons Instruments. Adsorption/desorption isotherms were performed at 77 K using N_2 as adsorbate. Specific surface area was calculated by the BET method[25] in a relative pressure range between 0.03 and 0.3. The pore size distribution was calculated using the method proposed by Barret, Joyner, and Halenda[26] on the desorption branch. Isotherms were classified using the IUPAC convention. Additionally, pure Aerosil OX-50 (100% by weight) was measured to compare the results for this with those obtained for the hybrid gels and the polymerized network (0% colloid by weight).

Results and Discussion

Figure 1 shows the curves obtained from mercury porosimetry experiments for encapsulated specimens and gels run without membrane. Samples containing 0% and 30% by weight of colloidal silica (Figure 1a,b) exhibited practically identical curves. This suggests that intrusion did not occur during the membrane-free run of the specimens, and thus the volume variation was exclusively due to gel strain under mercury pressure. Moreover, after tests, gel weight was not increased ($\Delta m < 0.2\%$, Table 1) and mercury traces did not appear, confirming that mercury was not intruded into gel network. However, when the silica powder proportion was increased (to 54, 65, and 82% by weight), a significant difference between the two curves is observed (Figure 1c−e, respectively). In each specimen run without rubber, the pressurization curve showed an abrupt change of slope (P_i in Figure 1), while the curves for encapsulated specimens, where intrusion was prevented, had a similar appearance to those containing a proportion of 0 and 30% of silica powder. In addition, specimens run free of rubber showed a substantial weight increase after test ($\Delta m > 48\%$, Table 1), exhibiting traces of trapped mercury. These results suggest that the significant change in curve slope is due to mercury intrusion into the gel network. Therefore, we consider the volume variation observed under pressure immediately below P_i to be related to the network shrinkage while

(25) Brunauer, S.; Emmett, P. H.; Teller, E. *J. Am. Chem. Soc.* **1938**, *60*, 309−319.
(26) Barret, E. P.; Joyner L. G.; Halenda, P. P. *J. Am. Chem. Soc.* **1951**, *73*, 373−380.

Table 1. Results from Porosimetry Curves[a]

	with membrane			without membrane			
colloid (wt %)	Δm (%)	V (mm^3/g)	V_R (%)	Δm (%)	V (mm^3/g)	V_R (%)	P_i (MPa)
0	0.20	75.04	44.5	0.00	76.03	42.5	
30	0.00	108.40	69.0	0.10	91.62	57.8	
54	0.10	192.94	52.0	48.20	229.67	65.3	56.4
65	0.00	269.16	55.6	51.75	367.82	70.1	41.3
82	0	391.30	38.6	50.90	527.43	70.8	32.7

[a] Δm is mass variation after test. V is volume variation at maximum pressure. V_R is retrieved volume after depressurization. P_i is intrusion pressure.

variation occurring above P_i is related to mercury intrusion in the pores that were not destroyed during the compression at lower pressures. Considering that the pores are interconnected, pressure outside the pores is counteracted by pressure exerted by the mercury inside the pores. Therefore, if network compression does occur, it must be low and it has not been taken into account.

From these findings, we use curves where intrusion did not occur (gel with silica powder content of 0% and 30% by weight and encapsulated specimens for higher contents) to provide information about strain behavior of gels under isostatic pressure of mercury. Although the gels produced in this paper are xerogels, the majority of existing studies on the strain behavior study of gels is based on aerogels. So, we compared our results with respect to those of aerogels,[27] where a linearly elastic deformation to small increases of pressure occurs, followed by a plastic hardening. Aerogels exhibit bulk modulus K, which is calculated from eq 2, where V is the volume of the sample and P is the pressure, constant in the elastic regime, whereas, in the plastic regime, K increases with volume according to a power law shown in eq 3, where K_0 and V_0 are the modulus and volume of the sample at the beginning of the power-law range, the exponent value being close to 3.

$$dP = -K(dV/V) \tag{2}$$

$$K(V) = K_0(V_0/V)^m \tag{3}$$

As shown in the curves of pressure versus volume (Figure 1), for each sample studied in this paper, a significant proportion of volume is not retrieved after the depressurization (Table 1), suggesting the irreversible nature of the strain that occurs during pressurization and, therefore, the plastic behavior of the materials. To calculate bulk moduli, curves of volume shrinkage (V/V_0) versus pressure (P) are plotted in Figure 2. As can be appreciated in the figure, the behavior of the xerogels studied did not correspond exactly to that reported for aerogels. Curves did not show the typical change in curvature attributed to the transition from elastic to plastic regime. Therefore, the yield point, which represents the limit of the elastic region, could not be distinguished.

The analysis of the curves obtained from the sequential compression experiment (the curve corresponding to 30% by weight colloid content is shown in Figure 3, as an example) gives an insight into the behavior of gels subjected to mercury isostatic pressure. All specimens exhibited an elastic response at lower pressures, which means that volume is fully retrieved after depressurization, until the pressure is increased beyond a determined value. From this point, the volume not retrieved increases progressively. This pressure was obviously associated with the yield point value. Results reported in Table 2 reveal that this value was progressively lower for gels containing

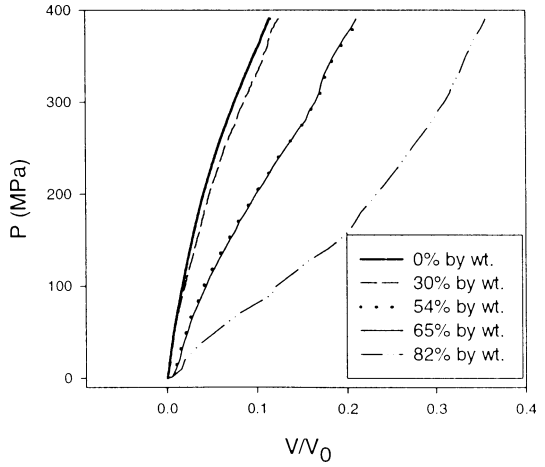

Figure 2. Compression curves obtained from mercury porosimetry tests where intrusion was prevented. V_0 is the initial volume of the sample.

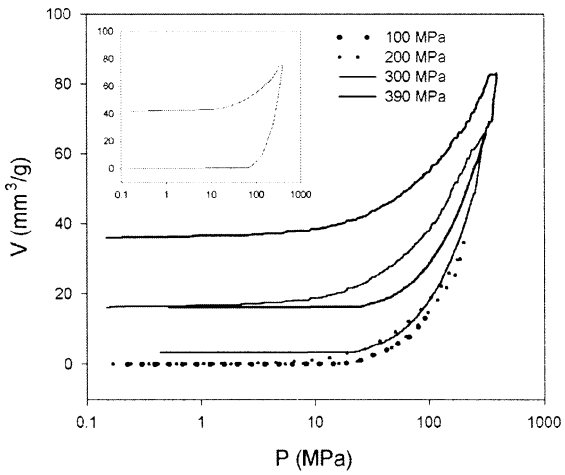

Figure 3. Curves of pressure vs volume from the sequential pressurization−depressurization experiment of a gel containing 30% by weight of silica colloid. Labels indicate the highest pressures reached in each cycle. The curve from a sample directly compressed to the highest pressure (390 MPa) is shown in the inset.

colloid in the range 0% to 54% by weight, remained constant for gels with 65% by weight, and was higher for the gel containing 82% by weight.

Knowing the yield pressure, we use data below this point for calculating bulk modulus corresponding to the elastic regime, which must be constant over the elastic area. Therefore, we determine this as the slope of the curve. As shown in Table 2, linear regression coefficients are above 0.99 for each gel, indicating that a Hookean strain is reached. A clear reduction of elastic modulus occurs when colloid content rises.

The bulk density of dried gel (Table 2) significantly decreased from 1.51 to 0.97 g/cm^3 when the silica content

(27) Scherer, G. W.; Smith, D. M.; Qiu, X.; Anderson, J. M. *J. Non-Cryst. Solids* **1995**, *186*, 316−320.

Table 2. Intrusion and Compression Results from Mercury Porosimetry[a]

		intrusion data		compression data		
colloid (wt %)	ρ_0 (g/cm^3)	P (%)	radius (nm)	ρ (g/cm^3)	yield (MPa)	K(MPa)
0	1.51			1.71	370	6032 (0.995)
30	1.36			1.55	300	5294 (0.991)
54	1.26	28.61	15.2	1.77	125	2686 (0.994)
65	1.11	41.65	20.7	1.41	125	2570 (0.993)
82	0.97	50.97	28.5	1.50	300	819 (0.993)

[a] ρ_0 is bulk density before compression. P is porosity. Radius is pore radius corresponding to maximum volume of mercury intruded. ρ is bulk density after compression. Yield corresponds to pressure where plastic strain is initiated. K is bulk modulus at elastic regime. Linear regression coefficients (r) are shown in parentheses.

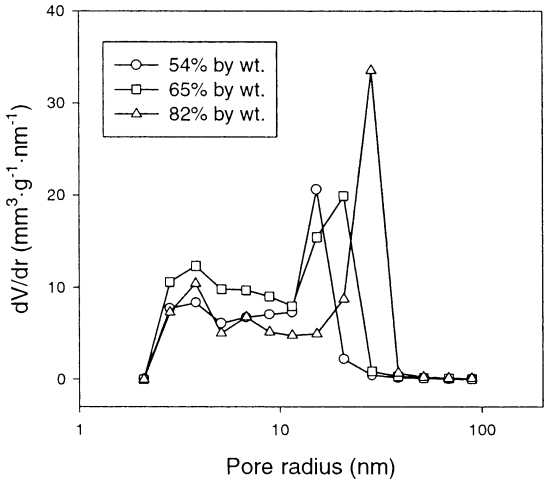

Figure 4. Pore radius distribution, obtained according Washburn interpretation, for pressures above P_i.

increased from 0 to 82% by weight. After specimen compression under mercury isostatic pressure, bulk density was clearly higher.

Concerning the textural properties of gels, we characterize pore structure from data above pressure P_i, according to the classical Washburn interpretation. As shown in Figure 4, pore radius distributions obtained were clearly bimodal. The progressive increase of silica particle content of the gel caused a gradual shift of pore radius corresponding to the maximum volume of mercury intruded, toward higher values (from 15 to 28 nm), while the peak of porous volume associated with lower values of pore radius remained practically constant. Porosity also increased from 28% to 51% (Table 2).

Figure 5 shows nitrogen adsorption−desorption isotherms. The pure TEOS gel (0% by weight) showed a sharp increase of adsorbed volume at P/P_0 below 0.1, followed by an almost horizontal adsorption over the whole pressure range and a final steep adsorption near saturation pressure. This feature is characteristic of the type I isotherm, which corresponds to microporous networks. By contrast, the isotherm of Aerosil OX-50 (100% by weight) exhibited a clear coincidence between adsorption and desorption branches, without any hysteresis loop appearing in the entire pressure range; this indicates that capillary condensation is not produced. This isotherm can thus be classified as type II, which is characteristic of nonporous solids or, as it may occur in this case, of macroporous solids. The high volume adsorbed at pressures close to saturation corroborates the presence of macropores. The high average pore size seems to indicate a poor aggregation between silica particles.

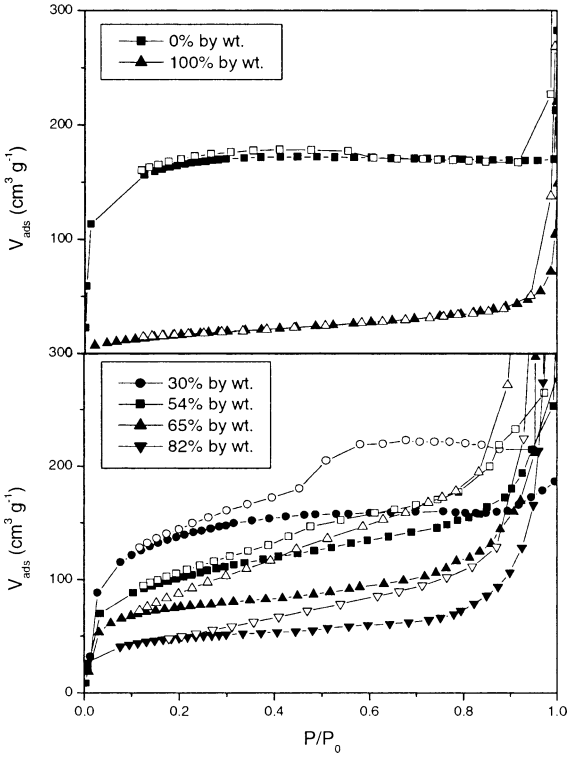

Figure 5. Nitrogen adsorption−desorption isotherms. Open symbols correspond to desorption branches.

On the other hand, gels containing proportions of colloid varying from 30 to 82% by weight exhibited type IV isotherms, which are characterized by clear hysteresis loops due to the capillary condensation, occurring in the mesoporous range. A clear transition is observed in the hysteresis loop from H4 to H3 type as silicate particles content is increased, revealing that colloid addition significantly modifies the pore structure of the gel network. Specifically, the gel containing the lower colloid proportion (30% by weight) showed a H4 hysteresis loop, which exhibits parallel and almost horizontal branches. This loop seems be merely due to the existence of mesopores formed by the xerogel on the surface of the silica particles, both of them embedded in the microporous xerogel matrix. In fact, the isotherm showed a sharp increase of adsorbed volume at low pressure, typical of microporous solids, thus corroborating the existence of this TEOS matrix. The gel containing 54% of silica retained some features of the H4 loop but began to feature the H3 type, which is characterized because saturation is not reached. It reveals a loose assemblage between particles and matrix, promoting the appearance of slitlike pores. Isotherms corresponding to 65% and 82% by weight of colloid content showed a clear H3 hysteresis loop, which indicates a tendency toward reduced aggregation between phases and, subsequently, toward an increase of the pore size.

As is shown in Table 3, textural properties exhibit a continuous evolution in line with the gradual increase of silica colloid content. Specific surface area progressively decreases from 492 to 157 m^2/g when the colloid proportion is increased from 0 to 82% by weight. Pore volume shows a tendency to increase with slight deviations, as colloid content is increased. For the gel containing 82% by weight of colloid, the pore volume value was more than twice that of the gel with 65% by weight Additionally, the mean pore radius and mean particle radius were calculated using a model of interconnected cylindrical pores and a model of homogeneous assembly of silica spheres, respectively.

Table 3. Experimental and Calculated Results from the Nitrogen Isotherms[a]

colloid content (wt %)	S (m^2/g)	V_p (cm^3/g)	R of pore (nm)	R of particle (nm)	coord no.
0	492	0.3286	1.34		10
30	392	0.2500	1.28	3.48	9
54	352	0.9751	5.54	3.87	8
65	251	0.6263	4.99	5.43	7
82	157	1.3481	17.17	8.69	6
100	66			20.66	

[a] S is specific surface area. V_p is porous volume. R of pore is average pore radius. R of particle is average particle radius assuming a model of silica spheres of 2.2 g/cm^3.

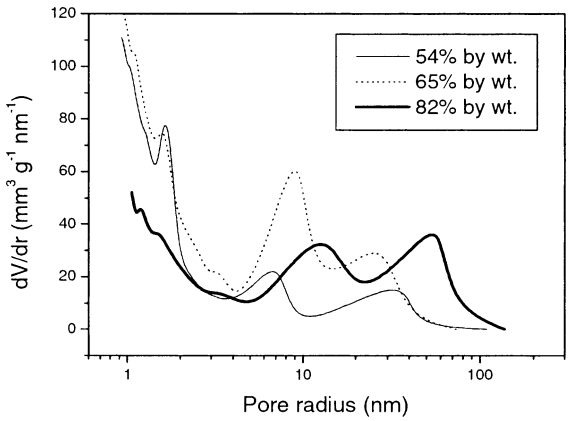

Figure 6. Pore radius distribution obtained from nitrogen adsorption isotherms.

Finally, the average coordination number n was calculated taking into account the equation proposed by Meissner:[28]

$$n = 2\exp(2.4\phi_s) \tag{4}$$

Here ϕ_s is the solid volume fraction as the ratio between the apparent density and the solid skeletal one (2.2 g/cm^3 as vitreous silica).

As Table 3 reveals, the radii of pores and particles progressively increase as colloid content increases. There is a noticeable and considerable increase of the average pore radius for the samples with the highest colloid content (from 5 nm, for the sample with 65% by weight to 17 nm for that with 82% by weight). With respect to the coordination number, this decreases when colloid content is increased, confirming the loosening of the aggregation previously conjectured.

Figure 6 shows pore radius distributions obtained from the isotherm data. The bimodality shown in the distribution obtained by mercury porosimetry (Figure 4) is again exhibited. By comparing specimens, we observe that the radius of pores shifts toward higher values as colloidal silica is increased. In contrast with the pore distribution in Figure 4, it is noticeable that there are micropores with pore radius below 2 nm, which is below the size limit that can be estimated by mercury porosimetry. Therefore, the pore volume values calculated by nitrogen adsorption (Table 3) are always higher than those obtained by mercury porosimetry (Table 2). This microporosity disappears for samples containing 82% by weight of colloid.

The next point in the discussion is to elucidate the behavior of gels subjected to mercury pressure. In the case of aerogels, it is well-known[27,29−31] that these are highly compliant materials, which are severely compressed when subjected to the mercury isostatic pressure, and all the pores of their network collapse. Therefore, mercury never intrudes into their pore structure. According to the following relationship,[32,33] intrusion pressure P_i is directly related to the compliance of the material, which is quantified by ratio between volume initial (V_0) and volume at this pressure (V), and is inverse to its pore radius (r_0).

$$P_i = \frac{2\gamma\cos\theta}{r_0}\frac{V_0}{V} \tag{5}$$

As a reduction in the compliance of a material implies a decrease of intrusion pressure, this explains why stiffer gels such as xerogels[34−37] and sono-aerogels[38] submitted to mercury porosimetry experience compression followed by intrusion. The specimens studied in this paper exhibit high modulus values (Table 2) that reveal the high degree of stiffness of their network. Therefore, intrusion occurrence is fully expected. On the other hand, the reduction of intrusion pressure as colloid content increase can be exclusively explained, in accordance with eq 5, as the consequence of a gradual increase of pore radius values, since a lower bulk modulus implies a higher material compliance. Textural data obtained by mercury porosimetry and nitrogen adsorption corroborate this increase of pore size.

Concerning the compression behavior of gels, analysis of the curves plotting volume versus pressure in samples where mercury is not intruded (Figure 1) shows that gels display an irreversible strain. In the case of aerogels:[30,31] the elastic deformation is the result of the contacts generated between solid parts, which where not initially in contact, while plastic strain is explained by the restructuring of the solid network. It seems proven that this irreversible modification is the consequence of the formation of siloxane bonds due to reactions of condensation between silanols, which still exist in TEOS aerogel. As the amplitude of shrinkage strongly depends on the fraction of porosity in the network, this stiffening mechanism occurs more rapidly when the gel is less dense.

We also observe a strong dependence between textural properties and strain behavior. Thus, the curves presented in Figure 2 indicate a progressive shrinkage of the gel as colloid content is increased. This is characterized by a progressive reduction of their bulk modulus. Concerning the limit of the elastic regime, this must be also progressively reduced. The sequential pressurization cycles confirm this, except for samples with the highest colloid content (82% by weight). The low proportion of TEOS in this specimen generates a low content in silanols, which makes the formation of siloxane bridges more difficult.

(28) Iller, K. *The Chemistry of Silica*; Wiley: New York, 1979; Chapter 5, p 462.

(29) Pirard, R.; Blacher, S.; Brouers, F.; Pirard, J. P. *J. Mater. Res.* **1995**, *10*, 2114−2119.

(30) Duffours, L.; Woignier, T.; Phalippou, J. *J. Non-Cryst. Solids* **1995**, *186*, 321−327.

(31) Woignier, T.; Duffours, L.; Beurroies, I.; Phalippou, J.; Delord, P.; Gibiat. V. *J. Sol-Gel Sci. Technol.* **1997**, *8*, 789−794.

(32) Scherer, G. W.; Smith D. M.; Stein, D. *J. Non-Cryst. Solids* **1995**, *186*, 309−315.

(33) Scherer, G. W. *Adv. Colloid Interface Sci.* **1998**, *76−77*, 321−329.

(34) Pirard, R.; Heinrichs, B.; Van Cantfort, O.; Pirard, J. P. *J. Sol-Gel Sci. Technol.* **1998**, *13*, 335−339.

(35) Alié, C.; Benhaddou, A.; Pirard, R.; Lecloux, A. J.; Pirard, J. P. *J. Non-Cryst. Solids* **2000**, *270*, 77−90.

(36) Alié, C.; Pirard, R.; Pirard, J. P. *J. Non-Cryst. Solids* **2001**, *292*, 138−149.

(37) Mosquera, M. J.; Pozo, J.; Esquivias, L. *J. Sol-Gel Sci. Technol.* **2003**, *26*, 1227−1231.

(38) Esquivias, L.; de la Rosa-Fox, N. *J. Sol-Gel Sci. Technol.* **2003**, *26*, 651−655.

The sequential pressurization cycles (Figure 3) reveals that, for pressures below the yield point, each curve is practically identical to that corresponding to the preceding pressure. However, beyond the yield point, the curve retraces the previous depressurization curve and in this pressure range matches perfectly that part of the curve corresponding to the sample compressed directly to the highest pressure. Thus, according to the idea of Scherer et al.,[27] the yield point may characterize the maximum pressure that the material has previously supported. If so, then it is clear that the yield point could be used to estimate the maximum capillary pressure to which the gel has been subjected during the drying.

In comparison, the decrease observed in yield point when colloid content increases suggests a clear reduction of capillary pressure. When the silica particle content is high, there are larger voids between particles, as was observed by nitrogen adsorption and mercury porosimetry; then according to Young−Laplace this must result in a reduction of capillary pressure. An exceptional behavior was exhibited by the gel containing 82% by weight, since the limit of its elastic regime is higher. The large pore size of the network, which reveals the existence of low capillary pressure, suggests that the specimen becomes stiff enough to support this pressure before the yield point can be reached. That is, this sample would experience a transient contraction as menisci form during drying and then recover completely as drying was completed. Therefore, in this specific case, the yield value cannot be associated with the capillary pressure.

It is important to note that cracking is due to the gradient in pressure rather than to the value of capillary pressure itself. Therefore, analysis of the permeability of the network could provide information on the pressure gradient that causes cracking. As permeability is proportional to the square of pore radius, we could initially assume that the addition of colloid generates an increase in the permeability of the network. However, loosening of the aggregation between silica particles and the TEOS matrix could significantly reduce its value. This could explain why, as Toki et al.[16] reported, gels containing colloidal silica of more 80% by weight suffered cracking during drying, while crack-free monoliths were obtained when the colloid content was within the range between 50 and 60% by weight. On the other hand, the loss of strength associated with the highest particle contents could also promote the appearance of cracking.

Conclusions

The addition of colloid silica particles to TEOS-based alcogels has enabled network porous volume and pore radius to be tailored, from a dense microporous material, such as the pure TEOS xerogel, into a mesoporous material with porosity increased up to 51%. Moreover, the increase in network pore size permitted a significant reduction of the capillary pressure during drying.

Additionally, possible direct relationships between textural parameters and the strain behavior of the gel were investigated. Increasing the colloid content resulted in a clear increase in the free volume of the network that amplified the gel shrinkage. The anomalous rise of the limit of elastic regime in gel with the highest proportion of colloid seems be caused by the reduction of TEOS content.

Acknowledgment. The authors are grateful for financial support from the Spanish Government: Ministerio de Ciencia y Tecnología (Projects MAT2001-3805 and MAT2002-0859). The authors are also grateful to Degussa Iberia, SA, for supplying Aerosil OX-50.

LA0265981